Author/s:
Bai, D;Huynh, MH;Simpson, DA;Reineck, P;Vahid, SA;Greentree, AD;Foster, S;Ebendorff-Heidepriem, H;Gibson, BC

Title:
Fluorescent diamond microparticle doped glass fiber for magnetic field sensing

Date:
2020-08-01

Citation:
Bai, D., Huynh, M. H., Simpson, D. A., Reineck, P., Vahid, S. A., Greentree, A. D., Foster, S., Ebendorff-Heidepriem, H. & Gibson, B. C. (2020). Fluorescent diamond microparticle doped glass fiber for magnetic field sensing. APL Materials, 8 (8), https://doi.org/10.1063/5.0013473.

Persistent Link:
https://hdl.handle.net/11343/252541

APL Materials

# Fluorescent diamond microparticle doped glass fiber for magnetic field sensing

Cite as: APL Mater. **8**, 081102 (2020); https://doi.org/10.1063/5.0013473
Submitted: 12 May 2020 . Accepted: 21 July 2020 . Published Online: 03 August 2020

D. Bai, M. H. Huynh, D. A. Simpson, P. Reineck, S. A. Vahid, A. D. Greentree, S. Foster, H. Ebendorff-Heidepriem, and B. C. Gibson

# Fluorescent diamond microparticle doped glass fiber for magnetic field sensing

Cite as: APL Mater. 8, 081102 (2020); doi: 10.1063/5.0013473
Submitted: 12 May 2020 • Accepted: 21 July 2020 •
Published Online: 3 August 2020



D. Bai,[1,a)] M. H. Huynh,[2] D. A. Simpson,[3] P. Reineck,[4] S. A. Vahid,[5] A. D. Greentree,[4] S. Foster,[6] H. Ebendorff-Heidepriem,[2] and B. C. Gibson[4]

## AFFILIATIONS

[1]School of Science, RMIT University, Melbourne, Victoria 3001, Australia
[2]The University of Adelaide, Adelaide, South Australia 5005, Australia
[3]School of Physics, The University of Melbourne, Victoria 3010, Australia
[4]ARC Center of Excellence for Nanoscale BioPhotonics, RMIT University, Melbourne, Victoria 3001, Australia
[5]School of Engineering, University of South Australia, Adelaide, South Australia 5095, Australia
[6]Defence Science and Technology Group, Edinburgh, South Australia 5111, Australia

[a)]**Author to whom correspondence should be addressed:** dongbi.bai@rmit.edu.au

## ABSTRACT

Diamond containing the nitrogen-vacancy (NV) center is emerging as a significant sensing platform. However, most NV sensors require microscopes to collect the fluorescence signals and therefore are limited to laboratory settings. By embedding micron-scale diamond particles at an annular interface within the cross section of a silicate glass fiber, we demonstrate a robust fiber material capable of sensing magnetic fields. Luminescence spectroscopy and electron spin resonance characterization reveal that the optical properties of NV centers in the diamond microcrystals are well preserved throughout the fiber drawing process. The hybrid fiber presents a low propagation loss of ~4.0 dB/m in the NV emission spectral window, permitting remote monitoring of the optically detected magnetic resonance signals. We demonstrate NV-spin magnetic resonance readout through 50 cm of fiber. This study paves a way for the scalable fabrication of fiber-based diamond sensors for field-deployable quantum metrology applications.



## I. INTRODUCTION

Negatively charged nitrogen-vacancy ($NV^-$) color centers in diamond have been extensively studied for precise magnetic field sensing,[1–4] quantum information technology,[5] as well as bio-medical thermometry and imaging.[6,7] As a sensor, the NV center can be optically addressed and manipulated remotely. Conventional NV sensing systems use either confocal[8,9] or widefield[10] collection of the fluorescence to provide rich information of their local (potentially nanoscale) environment. Nevertheless, the sophistication and lack of portability of such high-end microscopes have led to interest in integrating diamond NV centers with glass optical fibers. To date, the most commonly used approach to realize such a hybrid device relies on growing or placing diamond materials external to the fiber,[11–14] which enables $NV^-$ emitters to locate either on the endface of the fiber[15–17] or tapered fiber regions.[18–20] Diamond nanoparticles have been combined with tellurite (Te) glass to create hybrid diamond-glass fibers,[21] and Maayani *et al.* demonstrated distributed diamond-fiber magnetometry by periodically spacing photodiode chips along a polycarbonate clad silica fiber to detect the diamond-microfluidic systems configurated in the hollow fiber.[22]

Previously, we have employed a volume doping technique to integrate fluorescent diamond nanoparticles into the glass matrix, where the nanodiamonds (NDs) are dispersed into molten glass to create a ND-doped glass billet, which is subsequently processed using preform extrusion and fiber drawing to obtain an optical fiber with NDs distributed inside the whole fiber volume.[23,24] The volume doping approach has received remarkable progress in maintaining the single-photon emission[21,24] and optically detected magnetic resonance (ODMR)[25] properties of NV centers in fluorescent

NDs embedded in the fiber. However, the volume doping technique is challenging in terms of oxidization and dissolving of diamond nanoparticles during the doping step,[24,26] as well as achieving efficient excitation and collection of NV fluorescence via the fiber due to the absorption and scattering from diamond particles randomly distributed over the whole fiber cross section.

Here, we report a diamond-doped optical fiber made from lead-silicate glass using micrometer-sized NV-containing diamond crystals and a new doping method, which confines the diamond particles at an annular interface within the fiber cross section. The resultant fiber presents low loss and spatial confinement of NV fluorescence to the central region of the fiber geometry under laser illumination, which are favorable for fluorescence signal collection along the fiber. We performed magnetic field sensing in ambient environmental conditions via three different fluorescence excitation and collection architectures relative to the fiber axis. Bright photoluminescence from NV centers was obtained at the fiber output end, which leads to a fiber-based diamond-magnetometer with a sensing length up to 50 cm. The hybrid fiber also allows for the convenience of operation without easy breakage and promises the compatibility of the magnetically sensitive fiber with other fiber systems. Our results indicate that the microdiamond-doped lead-silicate glass optical fiber can be applied in versatile fiber platforms for remote sensing applications.

## II. RESULTS

We selected commercial F2 lead-silicate glass (Schott Glass Co.)[27] as the fiber material since this glass has a high mechanical stability and can be easily drawn into different structures without crystallization.[28,29] High-pressure high-temperature diamond particles with an average diameter of ~1 $\mu$m (MSY 0.75-1.25, Microdiamond, Switzerland) were used as dopants since such large particles offer a higher number of NV centers per particle and improved quality of the diamond host material compared to nanoscale diamond particles, which, in turn, leads to enhanced magnetic field sensitivity.[2,30]

Prior to fiber integration, the diamond particles were irradiated with 2 MeV electrons at a fluence of $1 \times 10^{18}$ cm$^{-2}$ followed by annealing (900 °C, 2 h) in argon to create NV centers. The particles were then oxidized in air (520 °C, 2 h) to remove non-diamond carbon from the particle surface. Based on measurements on bulk diamond samples that were processed analogous to the particles used here,[31] we estimate the NV center concentration in the diamond particle to be ~1 ppm. To examine the fluorescent emission properties of the diamond particles alone, we dispersed the processed diamond particles into ethanol to prepare a diamond solution with a concentration of ~0.4 mg/ml. The diamond solution was then spin-coated onto a glass cover slide. Figure 1(a) shows the confocal fluorescence image of the diamond particles on the glass substrate. The diamond particles are presented as fluorescent dots against the black background under 532 nm laser illumination. We examined 10 individual diamond particles, as labeled in Fig. 1(a). The average photoluminescence spectrum of the diamond particles was shown in Fig. 1(b), where the characteristic zero phonon line (ZPL) around 637 nm for NV$^-$ centers[1,2] can be clearly identified. The ODMR spectrum of the diamond particles was obtained by recording the NV$^-$ fluorescence intensity as a function of scanning microwave (MW) frequency. Figure 1(c) shows the average zero-field ODMR spectrum collected from the diamond particles, where the signature ODMR dip for NV$^-$ centers at ~2870 MHz is presented.[2]

Figure 2(a) illustrates our fiber fabrication steps, which followed a cane-in-tube approach.[28,32] First, a rod with an outer diameter (OD) of ~11 mm and a tube with an OD of ~9 mm and inner diameter (ID) of ~0.9 mm were made from ~30 mm diameter F2 glass billets using the extrusion technique.[32,33] Second, the rod was scaled down in size to an OD of ~0.6 mm using a drawing tower. Third, the surface of the rod was coated with diamond particles. To this end, the diamond solution as used above was shaken and sonicated for over 30 min to reduce the agglomeration of diamond particles. A dip coater was used in the coating process, which was set at a dipping/withdrawing speed of 200 mm/min. The remaining time of the rod in the diamond solution and the gap between

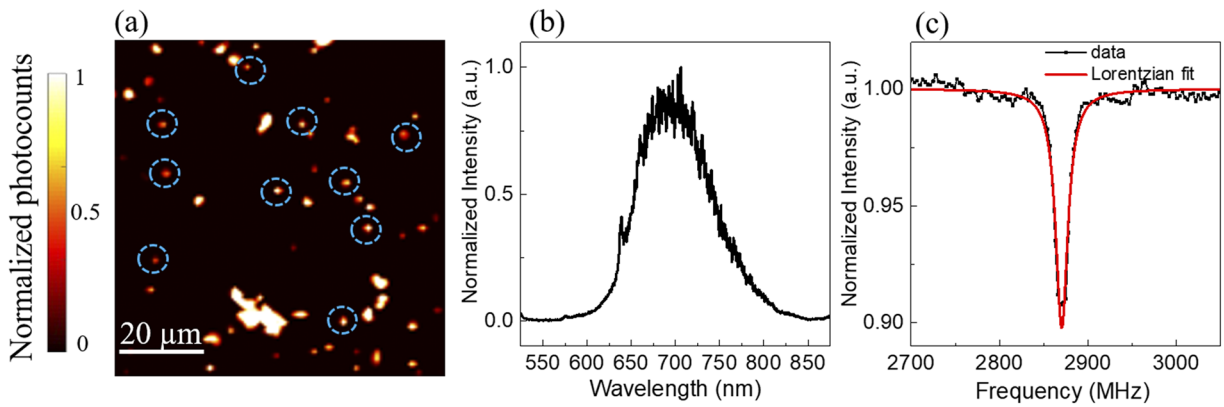


**FIG. 1**. (a) Confocal fluorescence mapping result of diamond particles deposited on a glass cover slide. The diamond particles were excited by a 532 nm continuous-wave laser, and the NV fluorescence emissions were collected by using a 532 nm notch filter. Dashed circles in the image denote the diamond particles we examined. (b) Average photoluminescence spectrum in the wavelength range of 525 nm–875 nm and (c) average ODMR spectrum at the zero magnetic field of the diamond particles. All signals were recorded at room temperature.

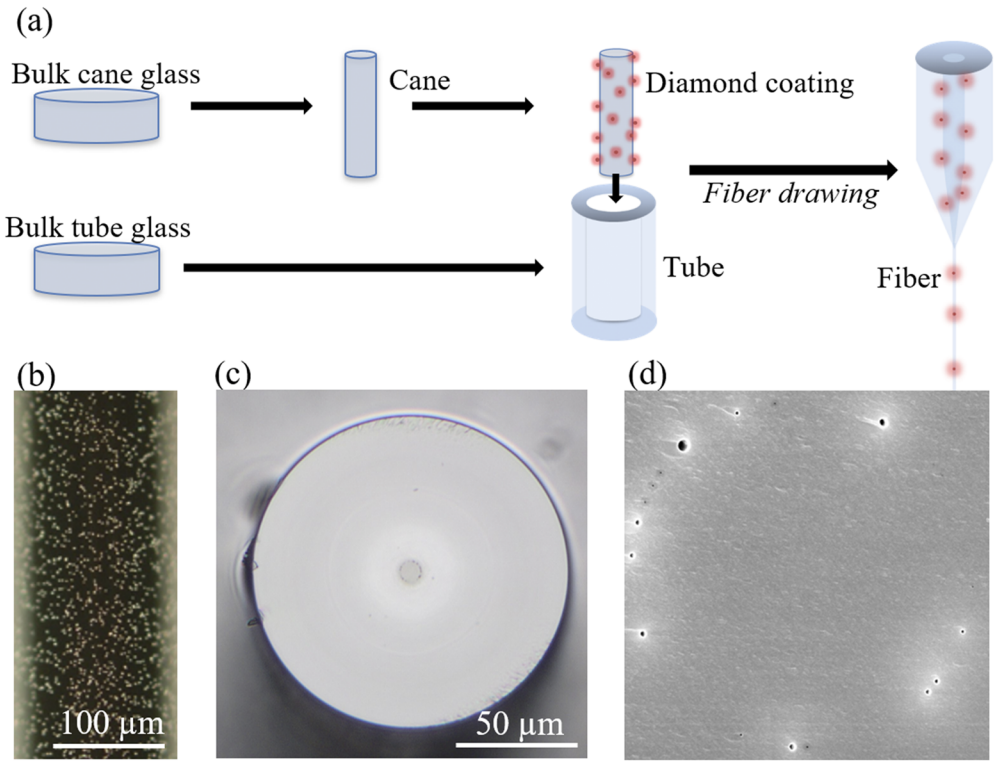


**FIG. 2**. (a) Illustration of the cane-in-tube fiber fabrication process. Two F2 glass billets were prepared. One billet was extruded into a tube. The other billet was extruded into a rod, which was drawn into a cane and coated with diamond particles. The coated cane was then inserted into the tube, and the cane-in-tube assembly was drawn down to the diamond-doped glass optical fiber. (b) Optical microscope image of the F2 glass cane coated with 1-$\mu$m microdiamond particles. Diamond particles are presented as white dots against the black background. The image was taken before the cane was inserted into the tube for fiber drawing by using a 20×, 0.45 numerical aperture objective. (c) Optical microscope image of the cross section of the diamond-doped F2/F2 fiber. The fiber presents an outer diameter of ~130 $\mu$m. Diamond particles are doped at the interface between the inner and outer fiber regions. The image was taken by a 20×, 0.4 numerical aperture objective. (d) Scanning electron microscopy image of the inner region of the diamond-doped F2/F2 fiber. The observed holes are due to the incomplete fusion of the F2 glass cane with the F2 glass tube in the fiber drawing process.

each dip were both 30 s. After 10–15 dips, the diamond solution was sonicated again for ~3 min to prevent the agglomeration and sediment of diamond particles in the solution. We implemented a total 25 dips in the coating process, which resulted in a relatively uniform distribution of diamond microparticles on the surface of the glass rod, as shown in Fig. 2(b). We found that further dipping would wash off the diamond particles and, in some cases, increase the agglomeration of particles. After coating, the glass rod was dried in air. Finally, the diamond-coated rod was inserted into the tube, and this preform assembly was drawn down to the fiber using a drawing tower. Reduced pressure was applied during fiber drawing to close the gap between the cane and the tube. From a single cane-in-tube assembly, over 100 m length of fiber was drawn. The cane (tube) part of the preform assembly leads to the inner (outer) region of the fiber. The diamond particles are distributed at the ring-shaped inner/outer interface within the fiber cross section. Hereafter, we refer to the fiber fabricated from the F2 cane and F2 tube as the F2/F2 fiber.

Figure 2(c) shows the cross-sectional optical image of the diamond-doped F2/F2 fiber. We took fiber samples from different bands of the fiber and measured the fiber OD and the diameter of the inner/outer fiber interface to be ~130 $\mu$m and ~9 $\mu$m, respectively. We observed tiny air holes at the fiber inner/outer interface, as shown in Fig. 2(d), from all bands of the drawn down F2/F2 fiber. To determine whether the air holes are caused by the embedded diamond particles, we fabricated an undoped F2/F2 fiber by using the same cane-in-tube preform parameters and fiber drawing conditions but without coating the cane. Similar interface hole features were shown in all sections of the undoped F2/F2 fiber. We note that the same effect of interface holes was observed for a step-index Te fiber, which was also made by the cane-in-tube technique with the cane and tube glasses having similar glass viscosity at the drawing temperature.[34] Therefore, we attribute the interface holes in the diamond-doped F2/F2 fiber to the fact that the F2 glass cane and F2 glass tube experienced the high and identical glass viscosity of ~$10^6$ dPa s during the fiber drawing process,[33] which causes incomplete fusion of the F2 glass cane with the F2 glass tube. For further comparisons, we also fabricated an unstructured undoped F2 fiber without any interface, where the extruded rod preform was directly drawn down to a fiber with ~160 $\mu$m diameter.

Figure 3 shows the measured loss spectra for the diamond-doped F2/F2 fiber, undoped F2/F2 fiber, and undoped unstructured

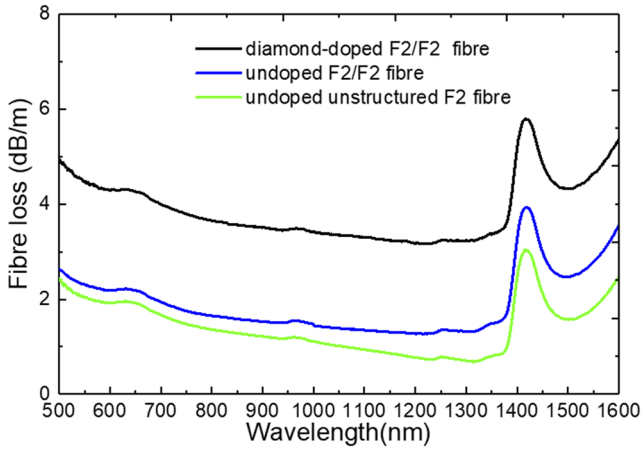


**FIG. 3**. Propagation loss of the diamond-doped F2/F2 fiber (black curve), undoped F2/F2 fiber (blue curve), and unstructured undoped F2 fiber (green curve) in the wavelength range of 500 nm–1600 nm. The relatively higher loss of the diamond-doped F2/F2 fiber is mainly due to scatterings induced by the diamond particles. Comparison between the two undoped fibers indicates that the interface holes have insignificant impacts on the fiber loss.

F2 fiber. The propagation loss at the excitation wavelength of 532 nm for NV fluorescence is higher for the diamond-doped F2/F2 fiber (~4.6 dB/m) compared to both the undoped F2/F2 fiber (~2.4 dB/m) and the undoped unstructured F2 fiber (~2.1 dB/m). Likewise, the propagation loss at the NV fluorescence emission wavelength range of 600 nm–800 nm is higher for the diamond-doped F2/F2 fiber (~4.0 dB/m) compared to the undoped fibers (~2.0 dB/m). The similar loss for the two undoped fibers indicates that the air holes at the inner/outer interface for the diamond-doped F2/F2 fiber induce only a small increase in fiber loss relative to the F2 fiber without interface holes. Therefore, the higher loss of the diamond-doped F2/F2 fiber relative to the undoped fibers is attributed to the micrometer-sized diamond particles at the inner/outer interface of the fiber.

We implemented three fluorescence excitation and emission collection schemes to examine the photoluminescent properties of the diamond-doped F2/F2 fiber. These configurations are shown in Fig. 4(a), which are side excitation (port A) with confocal collection (side/side scheme), side excitation (port A) with fiber endface (port B) collection (side/end scheme), and excitation from the proximal end (port C) with collection at the distal end (port B) of the fiber (end/end scheme). For all three schemes, the data were experimentally obtained from the same piece of the fiber sample. The fiber length from port A to B and port C to B was measured to be 20 cm and 50 cm, respectively. A continuous-wave (cw) 532 nm laser was employed as the excitation light, and the generated fluorescence for $NV^-$ centers was filtered out by using a combination of 532 nm notch filter and a 600 nm longpass filter. The three fluorescence excitation and collection schemes differ in their impact of fiber loss on the detected $NV^-$ fluorescence intensities as follows. For the side/side scheme, both the excitation and the emission of the $NV^-$ fluorescence experience negligible attenuation since they propagate only through a thin layer of glass (~50 $\mu$m) without diamond particles that would act as absorbing and scattering centers. For the side/end scheme, the $NV^-$ fluorescence generated at port A

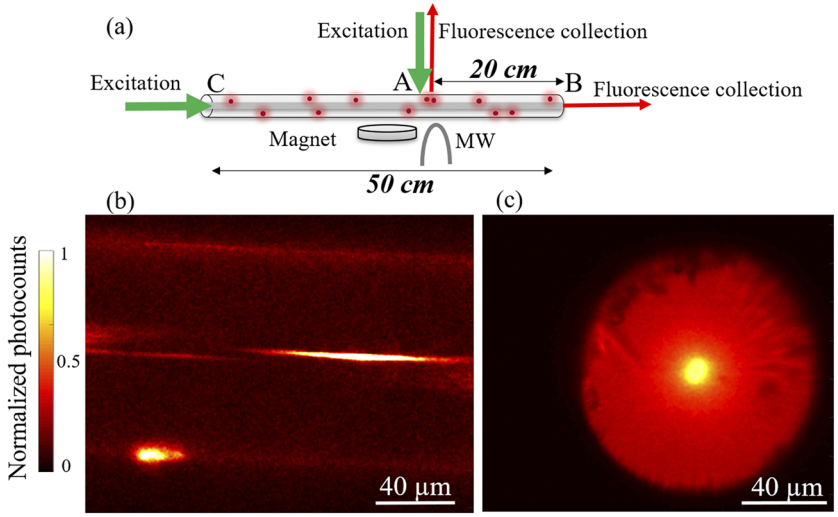


**FIG. 4**. (a) Schematic of fluorescence excitation and collection schemes for the diamond-doped F2/F2 fiber. In side/side scheme, the 532-nm continuous-wave laser was delivered from the fiber side (port A) with confocal fluorescence collection at the same site. In side/end scheme, laser excitation was delivered at port A, and fluorescence was collected at fiber endface (port B). In the end/end scheme, laser excitation was launched from the fiber proximal end (port C), and fluorescence was collected at the distal end (port B). For ODMR measurements, permanent magnets were used to vary the external magnetic fields. Microwave (MW) was provided by the antenna placed close to the fiber. [(b) and (c)] Fluorescence mapping result obtained from (b) the side of the fiber using the side/side scheme and (c) the endface of the using the side/end scheme. Bright spots in the central region of the fiber are fluorescent microdiamonds being confined at the fiber interface. The emitting spot on the outer edge of the fiber in (b) was caused by random dust/oil contamination, which can be eliminated by improving the fiber sample preparation process.

is affected by the attenuation through 20 cm of the fiber, whereas for the end/end scheme, both the excitation and the emission of the $NV^-$ fluorescence are affected by the attenuation through 50 cm of fiber.

Figure 4(b) shows the fluorescence map obtained from port A using the side/side scheme. The fluorescence is photostable with no blinking and is observed to originate from emitting particles located at the interface region of the F2/F2 fiber. Figure 4(c) corresponds to the fluorescence map recorded from port B by using the side/end scheme. In our study, we examined fiber pieces taken from all bands of the drawn F2/F2 fiber in different lengths and applied laser excitation either from the side or the proximal end of the fiber. Similar cross sectional fluorescence distribution was observed for every fiber sample. Based on the recorded fluorescence intensity as a function of location from the image, we determine that under laser illumination, the diamond-doped F2/F2 fiber delivers an averaged ~17% of the total NV fluorescence intensities via its fiber inner region over the entire fiber cross section. Meanwhile, the fiber outer region presents a radial spreading of the NV fluorescence where the fluorescence intensities gradually decrease from the inner/outer interface of the fiber to the outermost region of the fiber. We attribute that the spatial confinement of high-index diamond particles at the fiber inner/outer interface influences fluorescence guidance in the F2/F2 fiber. Specifically, due to the four allowed NV orientations within a single diamond microcrystal, the diamond particles embedded in fiber fluoresce approximately isotropically under laser excitation. The photons emitted toward the fiber inner region have a higher probability to scatter off other diamond particles and thus be gathered in the central region of the fiber.

In Fig. 5(a), we depict the photoluminescence spectra recorded from fluorescent spots in the F2/F2 fiber for three excitation/collection schemes. In all the measured spectra, the ZPL at 637 nm for $NV^-$ centers are clearly identified.[1,2] Compared to the spectrum observed for the side/side scheme, the spectra for the side/end and end/end schemes show a slight shift of NV fluorescence phonon sideband toward longer wavelengths. This is possibly due to scatterings and interferences from the diamond-doped fiber on the generated NV fluorescence when it transmitted through the fiber for photon collection at the fiber distal end. The spectral components around 550 nm observed for the end/end scheme are attributed to the Raman peaks for F2 glass under cw 532 nm laser excitation.[35] We note that proper optical filtering is essential to minimize the background noise for implementing the diamond-doped F2/F2 fiber in NV quantum sensing.

The magnetic field sensing behavior of the fiber was investigated based on the three excitation/collection schemes. Figure 5(b) shows the ODMR spectra obtained by launching excitation laser from port A and simultaneously collecting the $NV^-$ fluorescence as a function of MW frequency through the confocal setup via port A (black curve, side/side) as well as longitudinal transmission to the fiber end port B (blue curve, side/end). The ensemble of $NV^-$ centers

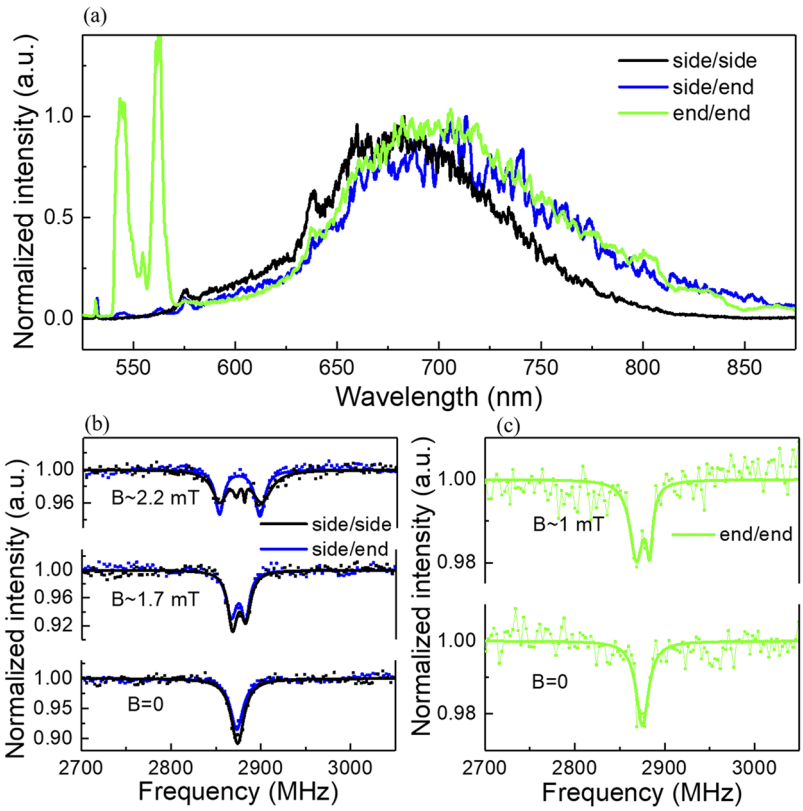


**FIG. 5**. (a) Photoluminescence spectrum in the wavelength range of 525 nm–875 nm recorded from fluorescent spots in different sensing schemes, confirming the NV centers in the diamond particles as the origin of the observed fluorescence in the F2/F2 fiber. The components around 550 nm from the end/end scheme are Raman peaks for the F2 glass under 532 nm laser excitation. (b) ODMR spectra measured at increasing external magnetic field B. Black curve: fiber side excitation/side collection; blue curve: fiber side excitation/end collection. (c) ODMR spectra recorded from the longitudinal end/end sensing scheme. In (b) and (c), dots are experimental data, and solid lines are Lorentzian fits.

in the microdiamond particle embedded in the F2/F2 fiber presents the signature ODMR dip at ~2870 MHz, which is further split by the Zeeman effect in the presence of an external magnetic field. The frequency transitions in the electron-spin resonance spectra thus provide the measurement of the vector components of the applied magnetic fields.[2,9] We note that the NV fluorescence spectrum and OMDR signals collected from localized characterization of the fiber [black curves for side/side scheme in Figs. 5(a) and 5(b)] are in good agreement with the results of the diamond particles alone [Figs. 1(b) and 1(c)], which proves that the optical and spin properties of NV centers in diamond particles are well preserved after embedding in the fiber.

Driven by the light transmission capability of the fiber, we also carried out the proof-of-concept experiment on remote diamond-magnetometry via the longitudinal end excitation/end collection fiber sensing scheme. Figure 5(c) shows the resultant ODMR spectra from the 50-cm fiber sample. The collected $NV^-$ fluorescence from the end/end scheme presents a read-out contrast of ~2.5% with MW frequency scanning. The splitting of the spectral lines is distinguishable under an external magnetic field strength of less than ~1 mT. However, we note that when a stronger magnetic field is applied, the spin-dependent fluorescence transmitted to the fiber distal end becomes masked by the background luminescence. This is mainly because in our current end/end scheme, the excitation beam was transmitted along the whole fiber sample, while the MW radiation was applied over the middle section of the fiber. Thus, the NV centers along the fiber, which do not experience the MW excitation, contribute to the systematic noise. To realize high-fidelity magnetic field readout via the remote sensing architecture, future study is required on reducing the fiber loss and optimizing the optical/MW interrogation on the tailored number of diamond particles along the fiber link.

We determine the current sensitivity of our diamond-doped F2/F2 fiber to DC magnetic fields by $\eta_{dc} \approx \Delta\nu/(\tilde{\gamma}_e C\sqrt{I_{PL}})$,[2,3,9] where $\Delta\nu$ is the full width half maximum (FWHM) linewidth of the ODMR dip, $\tilde{\gamma}_e \approx 2.8$ MHz/G is the electron gyromagnetic ratio, $C$ is the ODMR contrast, and $I_{PL}$ is the detected NV photoluminescence intensity under cw laser excitation. Considering the fiber loss, we experimentally detected a photoluminescence emission rate of $10^7$ counts/s, $5.5 \times 10^6$ counts/s, and $3.5 \times 10^6$ counts/s for ODMR signals obtained from the side/side, side/end, and end/end sensing scheme, respectively. As a result, the F2/F2 fiber demonstrates a room-temperature DC magnetic field sensitivity of 350 nT/$\sqrt{\text{Hz}}$ for localized NV-spin characterization (side/side scheme), 650 nT/$\sqrt{\text{Hz}}$ for a fiber transmission length of 20 cm (side/end scheme), and ~3 $\mu$T/$\sqrt{\text{Hz}}$ for longitudinally signal pumping and readout in a fiber length of 50 cm (end/end scheme).

We point out that the F2/F2 fiber achieves considerably enhanced magnetic sensitivity for hybrid diamond-doped glass optical fibers. As a comparison, the previously reported ND-doped Te fiber showed 10 $\mu$T/$\sqrt{\text{Hz}}$ sensitivity in a 5-cm side/end sensing scheme,[25] while in this study, the F2/F2 fiber showed over one order of magnitude higher magnetic field sensitivity in a 20-cm side/end sensing scheme. The sensitivity improvement demonstrated by the F2/F2 fiber is attributed to several following effects. In Table I, we further compare the relevant properties with the ND-doped Te fiber in Refs. 24 and 25.

### A. Diamond particle size

The F2/F2 fiber was doped with micrometer-size diamond particles (~1 $\mu$m). For magnetometry with NV defects in diamond, the shot-noise limited DC magnetic field sensitivity scales with $\sqrt{N_{NV}}^{-1}$, where $N_{NV}$ is the number of NV centers used in the sensing process.[2] Neglecting any agglomeration effects, the ~1 $\mu$m diamond particles used for the F2/F2 fiber offer about four orders of magnitude more NV centers than nanoscale diamond particles (~45 nm, as used in the Te fiber) due to their larger volume and therefore theoretically predict a ~100 times enhancement in the sensitivity (without taking fiber loss into account). Furthermore, for diamond particles above 100 nm in size, more NV centers are, in general, in the $NV^-$ state compared to smaller particles.[30,36] This is also important since only the $NV^-$ fluorescence is sensitive to magnetic fields.

### B. Doping geometry

The F2/F2 fiber was made using the interface doping method, where the diamond particles are spatially confined to the annular interface between the inner and outer regions. The interface embedding of diamond particles in fiber improves the optical transmission as evidenced by the lower loss of the doped F2/F2 fiber (~4 dB/m) relative to the doped Te fiber (~10 dB/m).[24] The comparison on fiber loss indicates that the spatial confinement of diamond particles compensates the larger scattering of the micrometer-scale diamonds

**TABLE I.** Comparison of the properties on fiber-based remote diamond magnetometry for the F2/F2 fiber in this study and the Te fiber in Refs. 24 and 25.

| Property | F2 | Te | F2 relative to Te | References |
|---|---|---|---|---|
| Diamond particles size | 1 $\mu$m | 45 nm | Larger size → higher NV density in excitation volume | 24 |
| Doping geometry | Interface | Volume | High spatial confinement → lower loss of fluorescence | 24 |
| Glass temperature during the doping step | 660 °C–690 °C | 610 °C | | 24 and 37 |
| Log viscosity (dPa s) during the doping step | 6.1–6.4 | 0 | Higher viscosity → lower chemical attack of diamonds | 38 and 39 |
| Refractive index contrast to silica[a] | 0.15 | 0.55 | Smaller index contrast → higher coupling | 24, 27, and 41 |
| Mechanical strength modulus (GPa) | 48 | 37 | Higher strength → higher robustness | 35 |

[a]Calculated at wavelength of 700 nm.

relative to smaller nanodiamonds. The lower loss of the F2/F2 fiber is also beneficial for increasing the number of photons collected from the fiber endface. In addition, the placement of NV emitters at the fiber inner/outer interface gathers the NV emission in the central region of the fiber waveguide, which further improves the fluorescence detection efficiency in the fiber-transmitted sensing scheme for enhanced ODMR sensitivity.

### C. Doping method

For the interface doping technique used for the F2/F2 fiber, diamond particles are embedded in the glass at the fiber drawing step. We determine that the F2 glass has a temperature of 660 °C–690 °C at the diamond doping step by using the offset between furnace temperature and glass temperature during the F2/F2 fiber drawing process.[37] Based on the Vogel–Fulcher–Tammann (VFT) temperature-viscosity relation for the F2 glass,[38] this F2 glass temperature was calculated to correspond to a glass viscosity of $10^{6.1}$ dPa s–$10^{6.4}$ dPa s, which confirms that the glass was softened but not molten at the diamond doping step. The relatively high F2 glass viscosity at the doping step reduces mass transport in the glass via convection and diffusion, which hinders the chemical reaction of the glass with the surface of the diamonds and/or dissolved gases in the glass. This property is essential to preserve the fluorescence emissions of NV centers in diamond particles embedded in the F2/F2 fiber, which leads to improved sensitivity in magnetic field sensing.

Moreover, our study proves the significance of the glass viscosity on the survival of nano/micro-crystals during the doping step. Comparing the interface doping for F2/F2 fiber and the volume doping for Te fiber, both the F2 and the Te glass were doped with diamond particles using similar doping time of 10 min–20 min.[24] We note that despite a slightly higher temperature at the interface doping step for the F2/F2 fiber (660 °C–690 °C) relative to the melt doping step for the Te fiber (610 °C), the diamond particles survived in the F2/F2 fiber due to the ~6 orders of magnitude higher viscosity for the F2 glass ($10^{6.1}$ dPa s–$10^{6.4}$ dPa s) during fiber drawing compared to the Te glass melt (~$10^{0}$ dPa s).[39] In accordance with the high viscosity, no evidence for dissolution of diamond particles was found for the interface doping of the F2 glass in this study, while strong diamond dissolution was found for the low-viscosity Te glass melt.[24] The critical effect of the glass viscosity at the diamond doping step is consistent with the observed increase in the dissolution of oxide nanocrystals in soft glass with increasing temperature.[40]

In addition, as shown in Table I, the use of F2 glass in this work shows the advantage in the integration of the magnetically sensitive fiber to silica fibers. The relatively low refractive index of the F2 glass (1.6) leads to better index-matching with silica glass (1.45),[27,41] which promises reduced Fresnel reflection and thus higher light transmission. Moreover, F2 glass shows a relatively high mechanical strength and low thermal expansion coefficient,[27] improving the mechanical robustness of diamond-doped fibers for practical applications.

## III. CONCLUSION

In summary, we have developed the design and manufacture of the intrinsic magnetically sensitive optical fiber by using lead-silicate glass, microdiamond particles, and the interface embedding technique. The diamond-doped fiber is investigated as a robust sensor that drives the fiber-optic magnetometry with ensemble NV centers in diamond. We achieve a room-temperature DC magnetic sensitivity of ~350 nT/$\sqrt{\text{Hz}}$ and ~650 nT/$\sqrt{\text{Hz}}$ by characterizing the NV-fluorescence captured from the fiber side and fiber output end, respectively. The fiber also facilitates ODMR readout via longitudinal laser initialization and signal collection along the fiber axis, leading to a current magnetic sensitivity of ~3 $\mu$T/$\sqrt{\text{Hz}}$ in a sensing length of 50 cm. The sensitivity of the fiber magneto-senor can be further enhanced by improving the purity of diamond particles with controlled nitrogen and carbon isotopes,[31,42,43] suppressing shot noise from the pump laser as well as magnetometry based on pulse quantum sensing and the lock-in detection scheme.[22,44,45]

We also conclude that the interface embedding is provided as an effective approach to incorporate photonic emitters into fiber channels, bringing up new opportunities to generate optical fibers for different sensing applications. Furthermore, our results highlight the need of fabricating diamond-doped fibers with the step-index core/clad structure, which yields potentially stronger coupling of NV fluorescence to guided fiber modes and precise quantification of magnetic fields in the longer sensing range. Our diamond-doped glass optical fiber can be expected to have significant impacts on quantum information science and persistent magnetic field monitoring applications.

## ACKNOWLEDGMENTS

This work was funded by the Defence Science and Technology Group under the Next Generation Technologies Fund (NGTF) program. Takeshi Ohshima and colleagues from QST, Takasaki, Japan, are acknowledged for irradiating the diamond samples. D.B. acknowledges Dr. Stephen Warren-Smith and Dr. Erik Schartner from the University of Adelaide for the fiber loss measurements and characterizations and Dr. Asma Khalid from RMIT University for the SEM imaging. A.D.G. acknowledges the Australian Research Council for financial support (Grant No. FT160100357). P.R. acknowledges funding through the RMIT Vice-Chancellor's Research Fellowship. This work was performed, in part, at the Opto-Fab node of the Australian National Fabrication Facility utilizing the Commonwealth and SA State Government funding.

## DATA AVAILABILITY

The data that support the findings of this study are available from the corresponding author upon reasonable request.

## REFERENCES

[1] M. W. Doherty, N. B. Manson, P. Delaney, F. Jelezko, J. Wrachtrup, and L. C. L. Hollenberg, Phys. Rep. **528**, 1 (2013).
[2] L. Rondin, J.-P. Tetienne, T. Hingant, J.-F. Roch, P. Maletinsky, and V. Jacques, Rep. Prog. Phys. **77**, 056503 (2014).
[3] G. Balasubramanian, I. Y. Chan, R. Kolesov, M. Al-Hmoud, J. Tisler, C. Shin, C. Kim, A. Wojcik, P. R. Hemmer, A. Krueger, T. Hanke, A. Leitenstorfer, R. Bratschitsch, F. Jelezko, and J. Wrachtrup, Nature **455**, 648 (2008).
[4] D. A. Simpson, R. G. Ryan, L. T. Hall, E. Panchenko, S. C. Drew, S. Petrou, P. S. Donnelly, P. Mulvaney, and L. C. L. Hollenberg, Nat. Commun. **8**, 458 (2017).

[5]S. Prawer and A. D. Greentree, Science **320**, 1601 (2008).
[6]G. Kucsko, P. C. Maurer, N. Y. Yao, M. Kubo, H. J. Noh, P. K. Lo, H. Park, and M. D. Lukin, Nature **500**, 54 (2013).
[7]L. P. McGuinness, Y. Yan, A. Stacey, D. A. Simpson, L. T. Hall, D. Maclaurin, S. Prawer, P. Mulvaney, J. Wrachtrup, F. Caruso, R. E. Scholten, and L. C. L. Hollenberg, Nat. Nanotechnol. **6**, 358 (2011).
[8]A. Gruber, A. Dräbenstedt, C. Tietz, L. Fleury, J. Wrachtrup, and C. von Borczyskowski, Science **276**, 2012 (1997).
[9]J. M. Taylor, P. Cappellaro, L. Childress, L. Jiang, D. Budker, P. R. Hemmer, A. Yacoby, R. Walsworth, and M. D. Lukin, Nat. Phys. **4**, 810 (2008).
[10]L. T. Hall, G. C. G. Beart, E. A. Thomas, D. A. Simpson, L. P. McGuinness, J. H. Cole, J. H. Manton, R. E. Scholten, F. Jelezko, J. Wrachtrup, S. Petrou, and L. C. L. Hollenberg, Sci. Rep. **2**, 401 (2012).
[11]S. Kuhn, C. Hettich, C. Schmitt, J.-P. Poizat, and V. Sandoghdar, J. Microsc. **202**, 2 (2001).
[12]J. R. Rabeau, S. T. Huntington, A. D. Greentree, and S. Prawer, Appl. Phys. Lett. **86**, 134104 (2005).
[13]T. van der Sar, E. C. Heeres, G. M. Dmochowski, G. de Lange, L. Robledo, T. H. Oosterkamp, and R. Hanson, Appl. Phys. Lett. **94**, 173104 (2009).
[14]E. Ampem-Lassen, D. A. Simpson, B. C. Gibson, S. Trpkovski, F. M. Hossain, S. T. Huntington, K. Ganesan, L. C. L. Hollenberg, and S. Prawer, Opt. Express **17**, 11287 (2009).
[15]T. Schröder, A. W. Schell, G. n. Kewes, T. Aichele, and O. Benson, Nano Lett. **11**, 198–202 (2010).
[16]I. V. Fedotov, S. M. Blakley, E. E. Serebryannikov, P. Hemmer, M. O. Scully, and A. M. Zheltikov, Opt. Lett. **41**, 472 (2016).
[17]D. Duan, G. X. Du, V. K. Kavatamane, S. Arumugam, Y.-K. Tzeng, H.-C. Chang, and G. Balasubramanian, Opt. Express **27**, 6734 (2019).
[18]T. Schröder, M. Fujiwara, T. Noda, H. Zhao, O. Benson, and S. Takeuchi, Opt. Express **20**, 10490 (2012).
[19]X. Liu, J. Cui, F. Sun, X. Song, F. Feng, J. Wang, W. Zhu, L. Lou, and G. Wang, Appl. Phys. Lett. **103**, 143105 (2013).
[20]R. N. Patel, T. Schröder, N. Wan, L. Li, S. L. Mouradian, E. H. Chen, and D. R. Englund, Light: Sci. Appl. **5**, e16032 (2016).
[21]M. R. Henderson, B. Gibson, H. Ebendorff-Heidepriem, K. Kuan, V. Afshar, J. Orwa, I. Aharonovich, S. Tomljenovic-Hanic, A. D. Greentree, and S. Prawer, Adv. Mater. **23**, 2806 (2011).
[22]S. Maayani, C. Foy, D. Englund, and Y. Fink, Laser Photonics Rev. **13**, 1900075 (2019).
[23]H. Ebendorff-Heidepriem, Y. Ruan, H. Ji, A. D. Greentree, B. C. Gibson, and T. M. Monro, Opt. Mater. Express **4**, 2608 (2014).
[24]Y. Ruan, H. Ji, B. C. Johnson, T. Ohshima, A. D. Greentree, B. C. Gibson, T. M. Monro, and H. Ebendorff-Heidepriem, Opt. Mater. Express **5**, 73 (2015).
[25]Y. Ruan, D. A. Simpson, J. Jeske, H. Ebendorff-Heidepriem, D. W. M. Lau, H. Ji, B. C. Johnson, T. Ohshima, S. A. Vahid, L. Hollenberg, A. D. Greentree, T. M. Monro, and B. C. Gibson, Sci. Rep. **8**, 1268 (2018).
[26]J. Zhao, X. Zheng, E. P. Schartner, P. Ionescu, R. Zhang, T. L. Nguyen, D. Jin, and H. Ebendorff-Heidepriem, Adv. Opt. Mater. **4**, 1507 (2016).
[27]See www.schott.com/advanced_optics/english/download/schott-optical-glass-collection-datasheets-july-2015-eng.pdf for Schott website for F2 glass.
[28]H. Ebendorff-Heidepriem, S. C. Warren-Smith, and T. M. Monro, Opt. Express **17**, 2646 (2009).
[29]Y. Ruan, H. Ebendorff-Heidepriem, S. Afshar, and T. M. Monro, Opt. Express **18**, 26018 (2010).
[30]P. Reineck, L. F. Trindade, J. Havlik, J. Stursa, A. Heffernan, A. Elbourne, A. Orth, M. Capelli, P. Cigler, D. A. Simpson, and B. C. Gibson, Part. Part. Syst. Charact. **36**, 1900009 (2019).
[31]M. Capelli, A. H. Heffernan, T. Ohshima, H. Abe, J. Jeske, A. Hope, A. D. Greentree, P. Reineck, and B. C. Gibson, Carbon **143**, 714 (2019).
[32]H. Ebendorff-Heidepriem and T. M. Monro, Opt. Express **15**, 15086 (2007).
[33]H. Ebendorff-Heidepriem and T. M. Monro, Opt. Mater. Express **2**, 304 (2012).
[34]S. Manning, Ph.D. thesis, University of Adelaide, November 2011.
[35]M. R. Bekteshi, M.Sc. thesis, University of Adelaide, May 2019.
[36]E. R. Wilson, L. M. Parker, A. Orth, N. Nunn, M. Torelli, O. Shenderova, B. C. Gibson, and P. Reineck, Nanotechnology **30**, 385704 (2019).
[37]M. J. Chen, Y. M. Stokes, P. Buchak, D. G. Crowdy, H. T. C. Foo, A. Dowler, and H. Ebendorff-Heidepriem, Opt. Mater. Express **6**, 166 (2016).
[38]Y. M. Stokes, P. Buchak, D. G. Crowdy, and H. Ebendorff-Heidepriem, J. Fluid Mech. **755**, 176 (2014).
[39]Unpublished data of temperature-viscosity dependence for 75 $TeO_2$-15 ZnO-10 $Na_2O$ (TZN) glass in studies of Refs. 22 and 23.
[40]J. Mrázek, H. Hesková, I. Kašík, L. Procházková, V. Čuba, E. Mihóková, and M. Nikl, paper presented at the 25th International Congress on Glass, Boston, MA, USA, June 2019.
[41]See https://www.heraeus.com/en/hca/products_hca/optical_fiber_1/preforms_1/preforms_fused_silica_hca.html for Heraeus website for fused silica glass.
[42]G. Balasubramanian, P. Neumann, D. Twitchen, M. Markham, R. Kolesov, N. Mizuochi, J. Isoya, J. Achard, J. Beck, J. Tissler, V. Jacques, P. R. Hemmer, F. Jelezko, and J. Wrachtrup, Nat. Mater. **8**, 383 (2009).
[43]T. Teraji, T. Yamamoto, K. Watanabe, Y. Koide, J. Isoya, S. Onoda, T. Ohshima, L. J. Rogers, F. Jelezko, P. Neumann, J. Wrachtrup, and S. Koizumi, Phys. Status Solidi A **212**, 2365 (2015).
[44]T. Wolf, P. Neumann, K. Nakamura, H. Sumiya, T. Ohshima, J. Isoya, and J. Wrachtrup, Phys. Rev. X **5**, 041001 (2015).
[45]H. Clevenson, M. E. Trusheim, C. Teale, T. Schröder, D. Braje, and D. Englund, Nat. Phys. **11**, 393 (2015).